Articles

Uncompetitive Antagonism of AMPA Receptors: Mechanistic Insights from Studies of Polyamine Toxin Derivatives

Trine F. Andersen,[†] Denis B. Tikhonov,[‡] Ulrik Bølcho,[#] Konstantin Bolshakov,[‡,||] Jared K. Nelson,[†] Florentina Pluteanu,[||] Ian R. Mellor,[||] Jan Egebjerg,[#,§] and Kristian Strømgaard[†,*]

Department of Medicinal Chemistry, The Danish University of Pharmaceutical Sciences, DK-2100 Copenhagen, Denmark, Sechenov Institute of Evolutionary Physiology and Biochemistry, Russian Academy of Sciences, St. Petersburg 194223, Russia, Department for Molecular Biology, University of Aarhus, DK-8000 Aarhus, Denmark, Division of Molecular Toxicology, School of Biology, University of Nottingham, Nottingham NG7 2RD, United Kingdom, and Division of Molecular Biology, H. Lundbeck A/S, DK-2500 Valby, Denmark

Received May 22, 2006

Philanthotoxins are uncompetitive antagonists of Ca^{2+}-permeable AMPA receptors presumed to bind to the pore-forming region, but a detailed molecular mechanism for this interaction is missing. Here a small library of novel philanthotoxins was designed and synthesized using a solid-phase strategy. The biological activities were investigated at cloned and "native" AMPA receptors using electrophysiological techniques. A distinct relationship between length of the polyamine moiety and the location of a secondary amino group was observed. Fitting the data to the Woodhull equation allowed the first experimental demonstration of the relative location and orientation of the philanthotoxin molecule in the receptor. These results were corroborated by in silico studies using a homology model of the AMPA receptor ion channel. Together these studies provide strong evidence for a molecular mechanism by which polyamine toxins antagonize the AMPA receptor ion channel and provide the basis for rational development of uncompetitive antagonists of AMPA receptors.

Introduction

In the mammalian brain, fast synaptic transmission is mainly mediated by glutamate binding to ionotropic glutamate (iGlu) receptors. This transmission underlies crucial brain functions including the molecular mechanism by which memories are formed and stored.[1−3] Moreover, dysfunction of iGlu receptors is implicated in a wide range of neurological insults including chronic neurodegenerative disorders such as Alzheimer's disease.[4−6]

The *N*-methyl-D-aspartate (NMDA) subtype of the iGlu receptors has attracted extensive attention due to its involvement in synaptic plasticity. Conventional competitive antagonists result in a complete block of activity, which leads to undesired effects; therefore development of uncompetitive antagonists, which only block activated receptors, is a more promising strategy. Recently, the promise of this strategy was shown, as memantine (Ebixa), a selective uncompetitive antagonist of NMDA receptors, was launched for the management of patients with moderate-to-severe Alzheimer's disease.[7] Another subtype of the iGlu receptors, the α-amino-3-hydroxy-5-methyl-4-isoxazolepropionate (AMPA) receptor, has recently been demonstrated to also be involved in synaptic plasticity.[8−11] Uncompetitive AMPA receptor antagonists are therefore believed to be useful in treating neurodegenerative disorders and/or reducing the amount of neurological damage associated with these disorders.[12−15] Thus, a detailed understanding of the mechanism by which uncompetitive antagonists of AMPA receptors work would allow for a more rational approach to the development of such compounds.

Low molecular weight polyamine toxins, isolated from venom of spiders and wasps, are a class of uncompetitive iGlu receptors antagonists.[16−18] The polyamine wasp toxin (*S*)-philanthotoxin-433 [(*S*)-PhTX-433, **1**; Figure 1] isolated from venom of the female digger wasp *Philanthus triangulum* is a prototypical example[19] that presumably binds inside the pore region of iGlu receptors. The use of philanthotoxins as templates for drug design has been hampered by their lack of selectivity toward specific receptors. But recently it has been demonstrated that modification of the polyamine portion of philanthotoxins led to an enhanced potency and selectivity at AMPA receptors.[20,21] Specifically, dicationic derivatives of **2**, such as **3** and **4** (Figure 1), were shown to be very potent and highly selective antagonists of AMPA receptors.[20,21]

Structurally, AMPA receptors are formed by homo- or heteromeric assembly of four subunits designated GluR1−4.[4,6] Each subunit is modular, containing a large N-terminal domain, a ligand-binding domain (LBD) and a transmembrane region, which forms the ion channel. The transmembrane region consists of three transmembrane domains (M1, M3, and M4), and a re-entrant loop (M2), that lines the narrow part of the ion channel. AMPA receptors can be classified according to their Ca^{2+} permeability; in GluR1, GluR3, and GluR4 a glutamine (Q) residue is present at a site known as the Q/R site located in the M2 segment of the AMPA receptor ion channel. This residue has been edited in virtually all GluR2 subunits to an arginine (R), which leads to a drastic reduction in Ca^{2+} permeability of AMPA receptors. This property is important as Ca^{2+}-permeable

* To whom correspondence should be addressed. Phone: +45 3530 6114. Fax: +45 3530 6040. E-mail: krst@dfuni.dk.
[†] The Danish University of Pharmaceutical Sciences.
[‡] Russian Academy of Sciences.
[#] University of Aarhus.
[||] University of Nottingham.
[§] H. Lundbeck A/S.

10.1021/jm060606j CCC: $33.50
Published on Web 08/09/2006

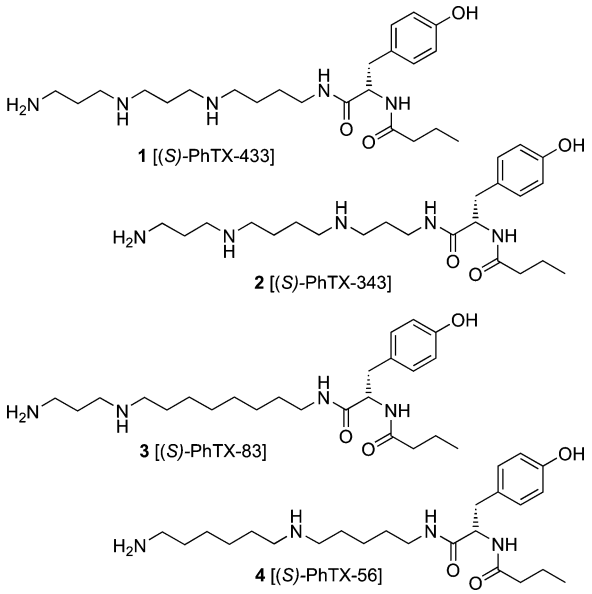

Figure 1. Structures of polyamine toxins. (*S*)-PhTX-433 (**1**) is the native philanthotoxin isolated from the wasp *Philanthus triangulum*, while compounds **2**, **3**, and **4** are derivatives, the latter being a very potent and highly selective AMPA receptor antagonist.

AMPA receptors are important for the pathogenesis of neurological disorders.[22] For example abnormal editing of GluR2 subunits, which leads to an increased number of Ca^{2+}-permeable AMPA receptors promotes amyotrophic lateral sclerosis (ALS) also known as Lou Gehrig disease.[23−25] Fortuitously, it is also the Ca^{2+}-permeable AMPA receptors that are highly sensitive to antagonism by philanthotoxin analogues, while those containing GluR2 subunits are almost insensitive. This enhances the therapeutic potential of these molecules.

In general, the iGlu receptor ion channels are structurally related to K^+-channels, though properties such as ion selectivtity are strikingly different.[26,27] Whereas several X-ray crystallographic structures of K^+ channels are known, no solid structural information is available for iGlu receptor ion channels.[26,28] Modeling studies of iGlu receptor ion channels, including the AMPA receptor, have been helpful in providing qualitative explanations for the differences in basic functions of these receptors[29] and the action of philanthotoxins and other cationic ligands. But the exact molecular mechanism by which philanthotoxins and related cationic compounds block iGlu receptors still remains to be validated. Here we have combined design and chemical synthesis of philanthotoxin derivatives with electrophysiological studies and molecular modeling to provide evidence for the mechanism of uncompetitive antagonism of iGlu receptors.

A number of studies have been carried out using PhTX-433 as a template.[20,21,30] The studies at Ca^{2+}-permeable AMPA receptors have provided highly potent and selective compounds, primarily dicationic derivatives such as **3** and **4**. Several studies have demonstrated that the polyamine portion of philanthotoxins is critical for specific interaction and seems to determine potency and specificity, whereas the tyrosine-*N*-butyramide moiety probably interacts in a more nonspecific manner but is important for anchoring the molecule to the receptor.[31] In most cases optimization of activity has focused on the number and position of the secondary amino groups, or the structure of the tyrosine-*N*-butyramide moiety,[16,17,31] while the distance of 12 atoms between the amide nitrogen and the terminal primary amino group has remained constant, reflecting the distance found in the native toxin, PhTX-433.

In this study, the design of novel derivatives transcends the dogma of a 12-atom distance based on the lead structure **4**. Two series of compounds were designed where either the distance between the secondary and primary amino groups was varied, (PhTX-5*n*, **10a**−**i**) or variation in the distance between the amide nitrogen and the secondary amine (PhTX-*n*6, **13a**−**g**) was performed. Thus the total distance between the amide nitrogen and the terminal primary amino group was varied between 8 and 18 atoms.

Results and Discussion

Synthesis of polyamines and polyamine toxins, in particular, has benefited tremendously from the use of solid-phase synthesis, the major advantage being that the tedious purification of highly polar intermediates is avoided and use of protecting groups is drastically reduced.[17,18] In particular, the Fukuyama amination has been a successful strategy for sequential synthesis of polyamines on solid-phase.[17,18] We have previously shown how a small library of polyamine toxins could be synthesized by a sequential strategy using Fukuyama amination, where an amine is protected and activated as a nitrobenzene sulfonamide, which is subsequently alkylated via a Mitsunobu reaction,[32] and the methodology has since been used for the synthesis of several philanthotoxin analogues.[20] The Fukuyama amination strategy[20,32] has been used to prepare the two series of compounds using parallel solid-phase synthesis, which in combination with automated, preparative LC-MS purification allows fast and efficient generation of the target compounds.

Preparation of philanthotoxin derivatives **10a**−**i** and **13a**−**g** is outlined in Figure 2. In brief, resin-bound diamines (**6a**−**i**) were reacted with *o*-nitrobenzenesulfonyl chloride to give the corresponding *o*-nitrobenzene sulfonamides (NS) **7a**−**i**. *N*-2-(Trimethylsilyl)ethoxycarbonyl (*N*-Teoc) protected amino alcohols **5a**−**h** were used as chain elongation fragments and were prepared from the appropriate amino alcohols as previously described.[20,32] The resin-bound *o*-nitrobenzene sulfonamides (**7a**−**i**) were reacted with the Teoc-protected amino alcohol building blocks (**5a**−**h**) in a modified Mitsunobu reaction, using 1,1′-(azadicarbonyl)-dipiperidine (ADDP) and tributylphosphine (Bu_3P) as redox reagents. Subsequently, the Teoc protecting group was selectively removed by treatment with tetrabutylammonium fluoride (TBAF) to give the resin-bound polyamine precursors **7a**−**i** and **11a**−**g**. These were reacted with (*S*)-Fmoc-*O*-(*tert*-butyl)tyrosine using HATU and collidine as coupling reagents, ensuring high (>99% ee) stereochemical purity. The Fmoc group was removed, followed by coupling with butyric acid and removal of the NS-group, before cleaving the compounds from the resin, with concomitant deprotection of the phenol to provide the compounds as crude products. These were purified by preparative HPLC-MS using intelligent fraction collection to provide the desired compounds, **10a**−**i** and **13a**−**g** in fair to good yields. All compounds were characterized by ^1H and ^{13}C NMR, as well as HRMS. Moreover, the purity of all compounds was assessed by HPLC with evaporative light scattering (ELS) detection. The latter is crucial for estimating purity, as ELS can detect polyamine impurities, which cannot be detected by conventional UV detection. All compounds were between 98 and 100% purity as determined by HPLC-ELS.

The biological activities of novel philanthotoxin derivatives **10a**−**i** (Figure 3a and 3d, and Table 1 in Supporting Information) and **13a**−**g** (Figure 3b and 3e and Table 2 in Supporting Information) were investigated in *Xenopus laevis* oocytes expressing either homomeric AMPA receptors composed of GluR1 subunits[20] or "native" AMPA receptors expressed from

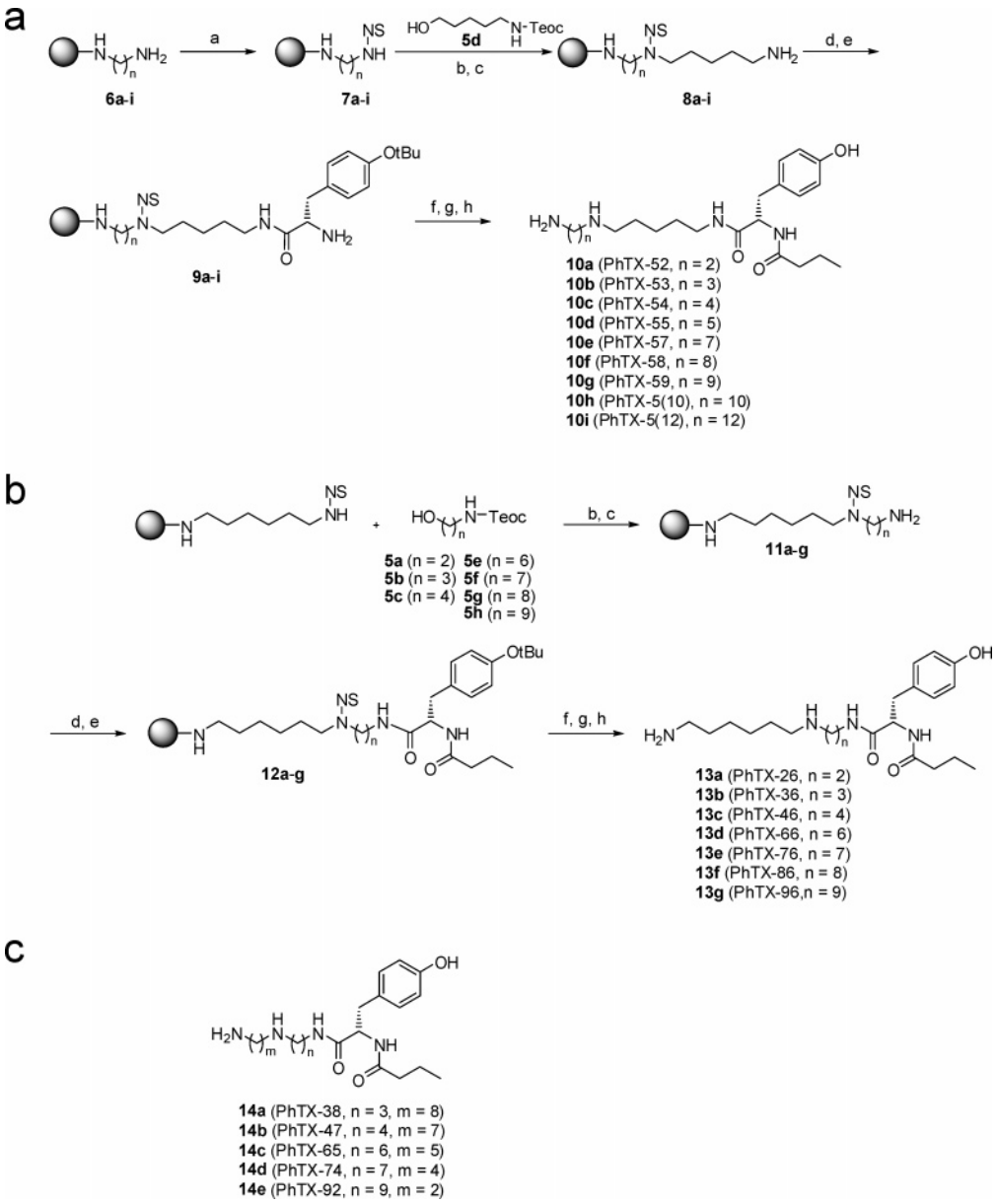

Figure 2. Synthesis of PhTX-5*n* and PhTX-*n*6 derivatives. (a) *o*-nitrobenzenesulfonyl chloride, DIEA; (b) 3-[*N*-[2-(trimethylsilyl)ethoxycarbonyl]-amino]alcohol, Bu_3P, ADDP; (c) TBAF; (d) (*S*)-*N*-Fmoc-*O*-(*tert*-butyl)tyrosine, HATU, collidine; (e) 20% piperidine in DMF; (f) butyric acid, HATU, collidine; (g) $HSCH_2CH_2OH$, DBU; (h) TFA, triisopropylsilane, CH_2Cl_2, H_2O.

whole rat brain RNA.[21] A two-electrode voltage clamp was used to measure the effect of the philanthotoxins on currents evoked by application of agonist (100 μM glutamate or kainic acid). All measurements were performed at a holding potential (V_H) of −80 mV unless otherwised stated. The oocytes were successively exposed to at least four concentrations of each toxin, and the resulting reductions in the amplitude of the agonist-induced current were used to derive IC_{50} values. In the case of cloned AMPA receptors, K_i values were estimated from IC_{50} values. We have previously synthesized PhTX-83 derivatives (**3**, **4**, **14a**−**e**, Figure 2c, Figure 3c and 3f and Table 3 in Supporting Information) and investigated those in the cloned AMPA receptor.[20] Here the biological activity of these derivatives at "native" AMPA receptors are described.

To rationalize the structure−activity profiles and to get an insight into a detailed molecular mechanism on uncompetitive antagonism of iGlu receptors, we combined the biological results with molecular modeling. Since there is no high-resolution structure available for the AMPA receptor ion channel, we needed to generate a homology model of this structure. Previously, a homology model of the AMPA receptor pore region was generated[33] based on homology with the K^+ channel from *Streptomyces lividans*, the KcsA K^+ channel that was crystallized and the structure solved.[34] This model predicts that the Q/R site (the selectivity filter) is situated at the mouth of the ion channel, and the Q/R site is stabilized by intersegment H-bonds.[29] A limitation of this model was the displacement of M2 segments from their positions in the template.[33]

In this study, a new homology model was created using the structure of the Ca^{2+}-gated K^+ channel from *Methanobacterium autotrophicum* (MthK) in its open form as a template.[35] Alignment of GluR1 and MthK sequences is unambiguous,[36] and to generate the homology model, an approach similar to that utilized for the Na^+ channel model was used,[37] i.e., the selectivity filter of the channel was shaped around the blocking compound, in this case the dicationic adamantane derivative **15** (Figure 4a). Constraints were imposed to preserve positions of the helical part of M2 (upstream from the Q/R site) and M3

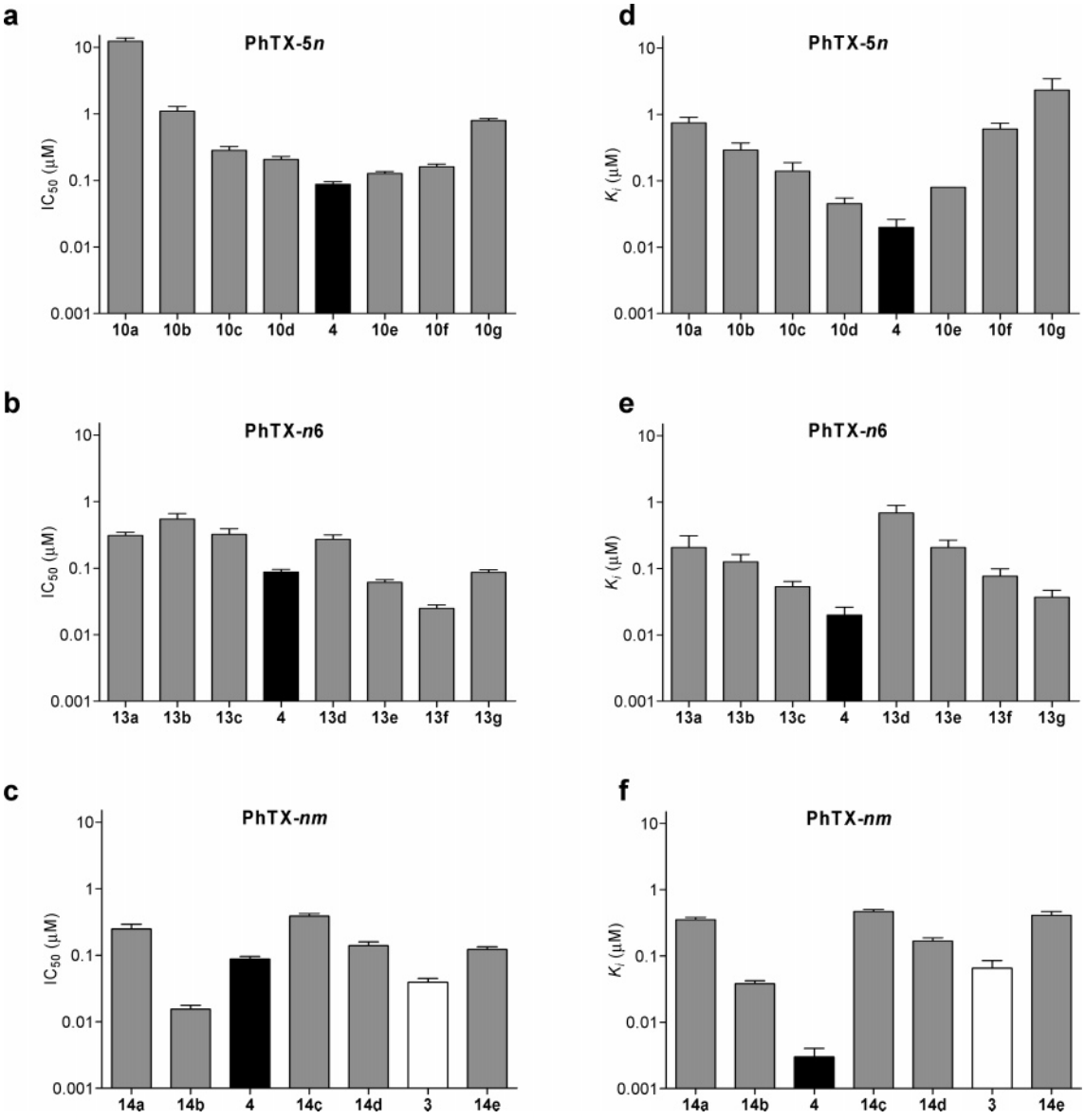

Figure 3. Biological activities of philanthotoxin derivatives investigated at "native" and cloned AMPA receptors. PhTX-5*n* derivatives showed a similar structure−activity profile when tested in (a) "native" and (d) cloned AMPA receptors, with the lead compound **4** being the most potent. The PhTX-*n*6 derivatives showed slightly different profiles at (b) "native" and (e) cloned AMPA receptors, where **4** was still the most potent in the latter type, the long-chain derivatives, particularly **13f** were more potent at "native" AMPA receptors. For the PhTX-83 derivatives a biphasic structure activity profile are observed at both (c) "native" and (f) cloned AMPA receptors. Whereas **4** is the most potent derivative at cloned AMPA receptors, **14b** is the most potent derivative at "native" receptors.

segments, as well as intersegment H-bonds in the Q/R site, and finally intensive Monte Carlo energy minimization generated the final model (Figure 4). The major advantage of this novel AMPA receptor ion channel model is the close similarity with K^+ channels, in particular, similar location of the M2 and M3 helical segments.

Generally, philanthotoxins are highly flexible structures, and their ligand-binding conformations are therefore not easily predicted. However, the energetically most favorable conformations of philanthotoxins correspond to closure of two intramolecular H-bonds between carbonyl oxygens and the secondary amino groups (forming the headgroup),[38] which provides a pronounced head-and-tail three-dimensional structure of philanthotoxins. Thus the size and the shape of the headgroup depends on the position of the secondary amino group and H-bonding.

First, the compounds were investigated in cloned and "native" AMPA receptors and generally a good agreement between the two receptor types was observed, with a noteworthy discrepancy (vide infra). In the PhTX-5*n* series (**10a**−**i**, Figure 3a and 3d; Table 1 in Supporting Information), compound **4** (IC_{50} = 87 nM; K_i = 20 nM) is the most potent compound and any change of the hexamethylene spacer between the secondary and primary amine decreases activity. Particularly the short chain compounds **10a** and **10b** show low activities and so does the very long chain derivative **10g**. Thus, these results suggest that the overall distance of 12 atoms between the amide nitrogen and the terminal primary amino group is optimal for activity.

In this series of compounds, modeling studies showed that only the distance between the headgroup and the terminal amino group is affected, whereas the overall head-and-tail conformation is not affected. The most potent compound in this series, compound **4** has a methylene spacer of $n = 6$, which reflects the distance between the hydrophobic (Q/R site) and nucleophilic (G+2)[39] components of the binding site. This is consistent

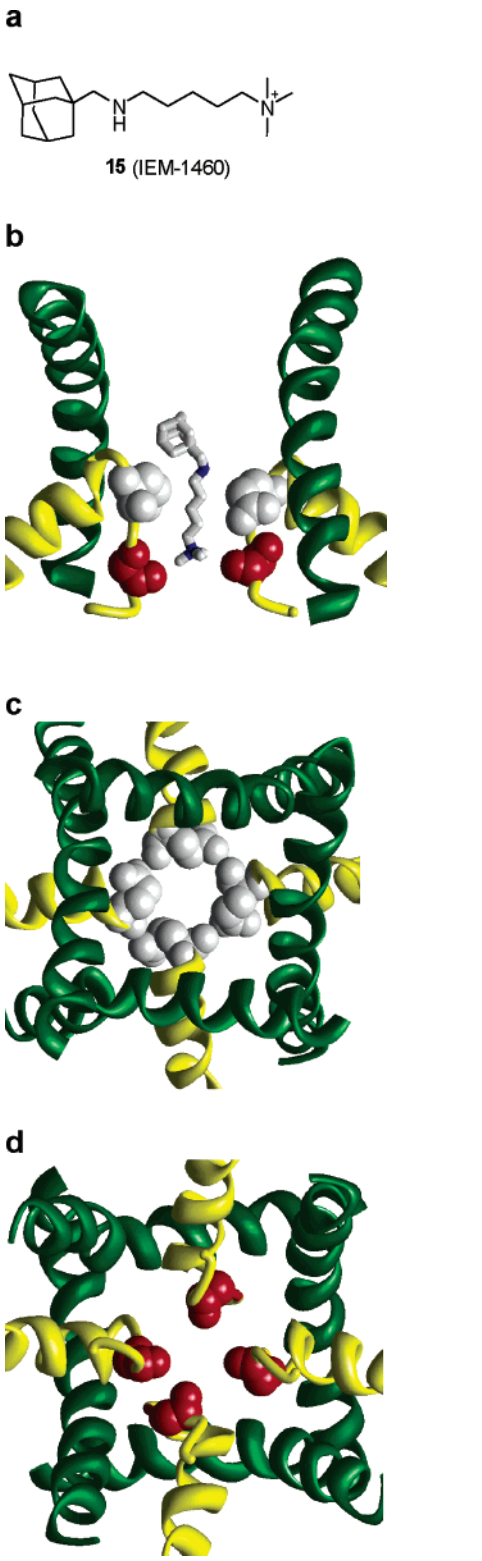

Figure 4. Homology model of the GluR1 AMPA receptor ion channel. (a) Chemical structure of compound **15**. (b) Side-view with compound **15** inside. (c) Extracellular view. (d) Intracellular view. M2 segments are yellow and M3 segments are green. Helical portions of the segments match the MthK template. The narrow part of the channel is shaped around **15**. Q residues at the Q/R site and G+2 residues are space filled in gray and red, respectively.

with experimental data obtained from dicationic derivatives of adamantine,[40,41] and thus, the homology model of the AMPA receptor ion channel and the head-and-tail conformation of philanthotoxins provide a rational explanation for observed biological data.

For the PhTX-*n*6 derivatives (**4**, **13a**−**g**, Figure 3b and 3e; Table 2 in Supporting Information), the biological results show a different structure activity profile at the two receptor types. At cloned AMPA receptors, the lead compound **4** (K_i = 20 nM) is still the most potent compound, but the slightly shorter derivative, **13c** (K_i = 53 nM), and the very long derivatives, **13f** (K_i = 77 nM) and **13g** (K_i = 37 nM), were all in the same range of activity. When tested at "native" AMPA receptors, the longer derivatives were ca. three times more potent than **4** (IC_{50} = 87 nM), the most potent compound being **13f** with an IC_{50} = 25 nM, thus being among the most potent uncompetitive antagonists described for AMPA receptors. Compounds **13e** (IC_{50} = 45 nM) and **13g** (IC_{50} = 86 nM) were, respectively, twice as potent and equipotent to **4**. The results from the PhTX-*n*6 derivatives suggest that the most important determinant for activity at both cloned and "native" AMPA receptors is the distance between the secondary and primary amino group, rather than the total distance of the polyamine moiety.

The modeling studies showed that in the PhTX-*n*6 series of compounds the hexamethylene spacer between the secondary and primary amino groups allows the terminal amino group to reach and bind to G+2, while the headgroup binds near the Q/R site. Thus, changes in biological activity originate from variation in dimensions and hydrophobicity of the headgroup. The narrow part of the channel pore can accommodate the headgroups of the short-chain derivatives **13a**, **13b**, **13c**, and **4**, and the difference in biological activity is explained by improved binding energy from increase in the headgroup size and hydrophobicity. Further increases in dimensions of the headgroup, as in **13d**, **13e**, **13f**, and **13g**, make it too big to fit the Q/R site and precludes simultaneous binding of the terminal amino group to G+2. However, **13f** and **13g** are still quite potent antagonists, which can be explained by their very flexible headgroups, which H-bond to form loops including 12 and 13 atoms, respectively. These headgroups can bind in the wide vestibule of the channel, above the Q/R site, providing superior interaction energy, thereby explaining their remarkable biological activity.

The derivatives of PhTX-83 (**3**, **4**, **14a**−**e**), where the distance of 12 atoms between the amide nitrogen and the terminal primary amino group has been kept constant and the position of the secondary amino group was varied, had previously been tested in the homomeric GluR1 AMPA receptor (Figure 3c and 3f; Table 3 in Supporting Information). These results showed that **4** was a very potent and highly selective antagonist of cloned AMPA receptors,[20] and their effect on "native" AMPA receptors was investigated. Similar to the previously described derivatives there was good agreement between the results obtained at the two different receptor types. In both cases a biphasic structure−activity profile was observed, but with a noteworthy discrepancy (Figure 3c and 3f; Table 3 in Supporting Information). At both receptor types, one peak of activity was found at compound **3** (IC_{50} = 39 nM and K_i = 65 nM). In cloned AMPA receptors, the second peak was found at compound **4** (K_i = 3 nM), whereas, in "native" AMPA receptors this peak was shifted along to compound **14d** (IC_{50} = 13 nM) which is ca. 5-fold more potent than **4** and the most potent antagonist at "native" AMPA receptors. This difference could be explained by differences in subunits of the two receptor types; the cloned receptor is made up of GluR1 flop subunits, whereas the "native" AMPA receptors contain GluR1, GluR3, and/or GluR4 in their flip or flop forms. The difference could also arise from the use

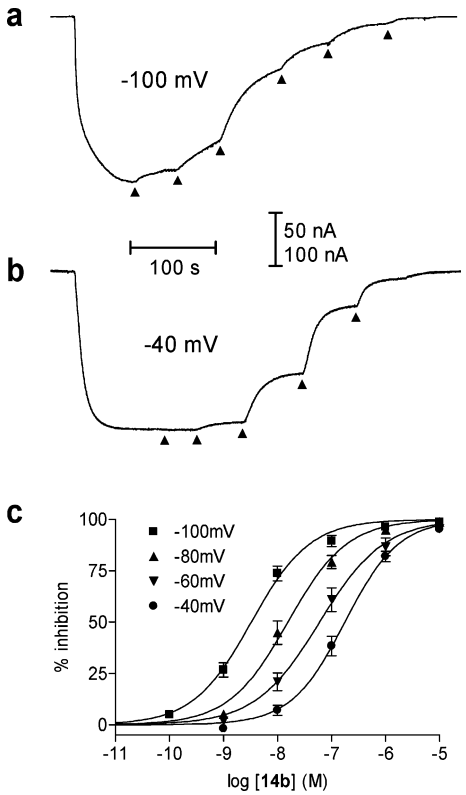

Figure 5. Voltage-dependent inhibition of responses to KA by **14b** in oocytes injected with rat brain RNA. (a and b) Currents in response to 100 μM KA at V_H of −100 mV (a) or −40 mV (b). **14b** (was added as indicated by the arrows in 10-fold increasing concentration steps of 10^{-10} M to 10^{-5} M at −100 mV or 10^{-9} M to 10^{-5} M at −40 mV. (c) Concentration−inhibition curves for antagonism of responses to 100 μM KA by **14b** at V_Hs of −40 mV (●), −60 mV (▼), −80 mV (▲), and −100 mV (■). Data points are mean %-inhibition ± standard deviation for n = 4, 5, 4−8, and 4−5 oocytes, respectively.

of different agonists glutamate and kainic acid, respectively, to activate the receptor, which might lead to slightly different conformations or opening times of the activated channel.

We investigated whether the activity of **14b** at "native" AMPA receptors was voltage-dependent, which would suggest an uncompetitive mode of action (Figure 5). A decreasing IC_{50} was seen at V_H = −100 mV (IC_{50} = 3.3 nM), while IC_{50} values were gradually increasing at −60 mV (IC_{50} = 60.1 nM) and −40 mV (IC_{50} = 176 nM). Thus, **14b** is a voltage-dependent antagonist of "native" AMPA receptors showing an open channel block of the AMPA receptor channel.

The peculiar biphasic structure−activity profile of the PhTX-83 derivatives (**3**, **4**, **14a**-**14e**) was evaluated in silico. The potent activity of **14b** and **4** is explained by the size of the headgroup and a favorable distance between headgroup and terminal amino group, as previously described. A similar conformation could not explain the potent activity of **3**, as the headgroup is too big and the polyamine tail too short in the H-bonded conformation. However, if **3** adopts an extended conformation, where both amino groups can interact with G+2, these H-bond/electrostatic interactions compensate for the loss of the internal H-bond and provide the high binding energy of **3** (Figure 6).

There has been much speculation about the orientation and relative location of the philanthotoxin molecule in the iGlu receptor ion channel; modeling studies have suggested that the aromatic headgroup is located at the entrance (Q/R-site) of the narrow part of the ion channel, while the polyamine tail binds oxygens from the backbone of the G+2 position[33,38] (Figure 6). Here we used an analysis of the series of PhTX-5*n*

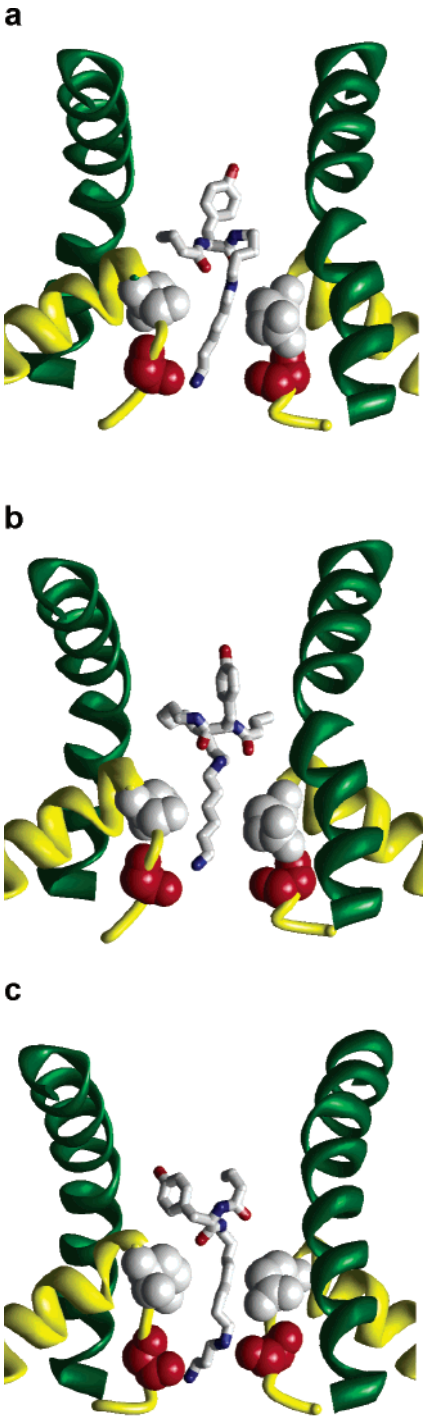

Figure 6. Docking of philanthotoxins to the GluR1 channel model. Optimal binding modes of (a) **4**, (b) **13g**, and (c) **3** are shown with two nonadjacent subunits. Headgroups interact with the Q/R site and with the M3 segments forming the walls of the channel vestibule whereas terminal amino groups bind to the G+2 oxygen ring. Compounds **4** and **13g** bind in the H-bonded conformation with the headgroup stabilized by intramolecular H-bonds. Compound **3** binds in extended conformation with both amino groups interacting with G+2 ring.

derivatives (**4**, **10a**−**i**) to experimentally prove the location and orientation of the molecule in the AMPA receptor ion channel. Philanthotoxins, which are cationic uncompetitive antagonists, are characterized by their dependence of activity on the transmembrane voltage (holding potential, V_H), as just described for **14b**. This voltage dependence can be used to estimate the relative position of the philanthotoxin binding site within the

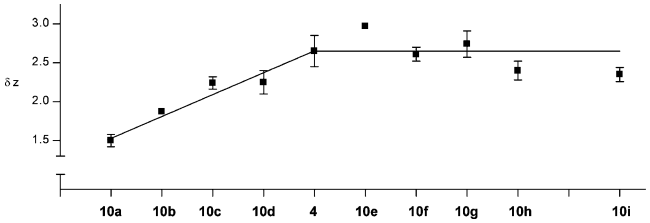

Figure 7. Determination of the location and orientation of philanthotoxins in the AMPA receptor ion channel. For compounds **10a** to **10i**, $z\delta$ values were calculated from estimated K_i values at V_H's of −60 mV, −80 mV, and −100 mV using Woodhull analysis. Since $z\delta$ is the sum of all charges times the fraction of the transmembrane voltage each charge senses at the binding site, the observed increase in $z\delta$ values for **10a**−**4** (sloping fit) implies that the terminal amino group binds deeper and deeper in the pore. For compounds **4**-**10i** (horizontal fit) the $z\delta$ values are on the same level indicating that the terminal amino group has reached the cytoplasm. Data points are mean ± standard deviation for $n = 4-6$ oocytes, respectively.

transmembrane electric field using the Woodhull equation, eq 1.[42]

$$\log K_i = \log K_{i0} + (z\delta \times FV/2.303 \times RT) \qquad (1)$$

Hence, analysis of the voltage dependence for a homologous series of philanthotoxins, such as the PhTX-5*n* derivatives (**4**, **10a**−**i**), can be used to impart information on the binding mode of these compounds. This requires determination of IC_{50} values and estimation of K_i values for each of these compounds at different holding potentials (V_H), followed by calculation of $z\delta$ values using the Woodhull equation where z is the valence of the compound and δ is the fraction of the electric field experienced by the compounds, as calculated from K_i and V_H.[42]

Therefore we determined IC_{50} values and subsequent estimation of K_i values for the PhTX-5*n* derivatives (**4**, **10a**−**i**) at three different holding potentials, $V_H = -60$, −80, and −100 mV, respectively. Then $z\delta$ values were calculated and plotted against the interamine distance (Figure 7), and it is observed that the $z\delta$ values increase monotonically for compounds **10a**−**4** while they saturate for compounds **4**−**10i**.

The increase in $z\delta$ values implies that the terminal amino group binds deeper and deeper in the pore, and that the aromatic headgroup is fixed, while the saturation indicates that the terminal amino group of these compounds penetrates the entire channel and reaches the internal side of the membrane. Together this leaves only one possible mode of binding: The aromatic headgroup is fixed at the channel narrowing (Q/R-site) and the polyamine tail penetrates the channel. This has been proposed on the basis of modeling studies[33,38] (see Figure 6), but here the relative location and orientation of philanthotoxins bound in the AMPA receptor ion channel is demonstrated experimentally for the first time.

Conclusion

Rational design of uncompetitive antagonists of iGlu receptors requires an understanding of the molecular mechanisms by which these compounds interact with the receptor. The present study uses a combination of chemical synthesis, molecular biology, electrophysiology and molecular modeling to provide a detailed view of how polyamine toxins interact with Ca^{2+}-permeable AMPA receptors and supports the view that the AMPA receptor channel binding site is composed of hydrophobic and nucleophilic components. The results will be important for the future developments of uncompetitive ligands for iGlu receptors and for the development of novel treatments for diseases in the brain.

Experimental Section

Chemistry. General Procedures. Resin-bound diamines (trityl chloride resin, 1% divinylbenzene, 200−400 mesh) and (*S*)-Fmoc-*O*-(*tert*-butyl)tyrosine were obtained from Novabiochem (Läufelingen, Switzerland). All other starting materials were obtained commercially from Aldrich or Fluka. All starting materials and solvents were used without further purification except DMF, which was stored over 3 Å molecular sieves and THF, which was distilled under N_2 from Na/benzophenone. All reactions on solid phase were carried out using MiniBlock (Mettler Toledo, Columbus, OH). ^{1}H NMR and ^{13}C NMR spectra were recorded on a Varian Mercury spectrometer at 300 MHz or on a Varian Gemini 200 BB at 300 MHz, using $CDCl_3$ or CD_3OD as solvents. Chemical shifts are reported in ppm (δ). Coupling constants (J) are given in Hz. Multiplicities of ^{1}H NMR signals are given as follows: s, singlet; bs, broad singlet; d, doublet; t, triplet; dt, doublet of triplets; q, quartet; p, pentet; m, multiplet. Analytical and preparative high-performance liquid chromatography (HPLC-MS) was performed on a Sciex API150ex instrument equipped with Atmospheric Pressure Chemical Ionization (APCI) ionsource. The HPLC system consisted of two Shimadzu LC10ADvp pumps. UV traces were obtained with a Gilson UV/VIS 155 UV detector operating at 254 nm. Evaporative light scattering (ELS) traces were obtained with Sedere Sedex 55 Light Scattering Detector and were used for estimation of the purity of the final products. Analytical HPLC-MS was performed on a 50 × 4.6 mm YMC RP18 column, using 2 mL/min of a mixture of A: water with 0.05% TFA and B: acetonitrile with 5% water and 0.035% TFA. Preparative HPLC-MS (split-flow MS detection) was run with 500 μL injections (20 mg samples in 1.0 mL DMSO) to a Phenomenex Synergi Hydro 4 μm, 21.20 × 50 mm column eluted with the same solvent gradient at 22.7 mL/min. Accurate mass determination was performed on a JEOL JMS−HX110/100A HF mass spectrometer using a 3-nitrobenzyl alcohol (NBA) matrix and Xe ionizing gas, and all were within ± 5 ppm of theoretical values.

Preparation of *N*-(Trimethylsilyl)ethoxycarbonyl Amino Alcohols (5a−h). The compounds were prepared as previously described.[20]

Synthesis of PhTX-56 Analogues (10a−i, 13a−g). General Procedure. Resin-bound diamines (0.16 mmol) were suspended in CH_2Cl_2 (4 mL). Diisopropylethylamine (DIEA) (0.96 mmol) and *o*-nitrobenzenesulfonyl chloride (0.64 mmol) were added successively, and the reaction mixture was stirred under nitrogen at room temperature for 3 h. The resin was drained and washed with DMF (3 × 2.5 mL), CH_2Cl_2 (3 × 2.5 mL), MeOH (3 × 2.5 mL), and CH_2Cl_2 (3 × 2.5 mL) and dried in a vacuum. The above resin was suspended in dry THF/CH_2Cl_2 (1:1) (2 mL) under nitrogen. A solution of a *N*-Teoc amino alcohol (0.8 mmol) in dry THF/CH_2Cl_2 (1:1) (1 mL), tributylphosphine (0.8 mmol), and a solution of 1,1′-(azadicarbonyl)-dipiperidine (ADDP) in dry THF/CH_2Cl_2 (1:1) (1 mL) were added successively. The mixture was stirred at room temperature under nitrogen for 3 h. The resin was drained and washed with DMF (3 × 2.5 mL), CH_2Cl_2 (3 × 2.5 mL), MeOH (3 × 2.5 mL), and CH_2Cl_2 (3 × 2.5 mL) and dried in a vacuum. The procedure was repeated two more times, and the resulting resin was dried in a vacuum. The above resin was suspended in dry THF (5 mL) under nitrogen at 50 °C. A solution of TBAF (1 M in THF, 0.64 mmol) was added slowly, and the mixture was stirred at 50 °C for 30 min. The resin was drained and washed with DMF (3 × 2.5 mL), CH_2Cl_2 (3 × 2.5 mL), MeOH (3 × 2.5 mL) and CH_2Cl_2 (3 × 2.5 mL) and dried in a vacuum. A solution of (*S*)-*N*-Fmoc-*O*-(*tert*-butyl)tyrosine (0.48 mmol) and HATU (0.48 mmol) in DMF (1 mL), followed by a solution of collidine (0.72 mmol) in DMF (0.5 mL) was added to the resin. The mixture was stirred at room temperature for 2 h, and the resin was subsequently washed with DMF (3 × 2.5 mL), CH_2Cl_2 (3 × 2.5 mL), MeOH (3 × 2.5 mL) and CH_2Cl_2 (3 × 2.5 mL). The product was treated with 20%

piperidine in DMF (v/v, 2 mL), and the mixture was agitated for 3 min at room temperature. The resulting resin was washed with DMF (3 × 2.5 mL), treated again with 20% piperidine in DMF (v/v, 2 mL) for 20 min, washed with DMF (3 × 2.5 mL), CH_2Cl_2 (3 × 2.5 mL), MeOH (3 × 2.5 mL), and CH_2Cl_2 (3 × 2.5 mL), and dried in a vacuum. A solution of butyric acid (0.48 mmol) and HATU (0.48 mmol) in DMF (1 mL), followed by a solution of collidine (0.72 mmol) in DMF (0.5 mL), was added to the resin. The mixture was agitated at room temperature for 2 h. The resin was drained and washed with DMF (3 × 2.5 mL), CH_2Cl_2 (3 × 2.5 mL), MeOH (3 × 2.5 mL), and CH_2Cl_2 (3 × 2.5 mL) and dried in a vacuum. The resin was treated with DBU (0.6 mmol) in DMF (1 mL) and mercaptoethanol (0.6 mmol) in DMF (1 mL) for 30 min. The resin was drained and washed with DMF (5 × 2.5 mL). The procedure was repeated three more times. The resin was washed with DMF (3 × 2.5 mL), CH_2Cl_2 (3 × 2.5 mL), MeOH (3 × 2.5 mL), and CH_2Cl_2 (3 × 2.5 mL) and then treated with a solution of CH_2Cl_2/TFA/triisopropylsilane/H_2O (47.5:47.5:2.5:2.5 v/v, 2 mL) for 2 h. The resin was drained and washed with MeOH (2 mL) and CH_2Cl_2 (2 mL). The solutions of the cleaved product and the washings were combined and evaporated in a vacuum and purified by preparative HPLC-MS to give the final products.

(*S*)-*N*-[5-[(2-Aminoethyl)amino]pentyl]-4-hydroxy-α-[(1-oxobutyl)amino]benzene-propaneamide Bis(trifluoroacetate) (PhTX-52, 10a). Yield: 18%. ^{1}H NMR (CD_3OD): δ 0.86 (t, J = 7.3 Hz, 3H), 1.20−1.72 (m, 8H), 2.17 (t, J = 7.1 Hz, 2H), 2.79 (dd, J = 13.6/8.1, 1H), 2.92−3.22 (m, 9H), 4.43 (t, J = 7.7 Hz, 1H), 6.69 (d, J = 8.5 Hz, 2H), 7.04 (d, J = 8.5 Hz, 2H). ^{13}C NMR: δ 13.9, 20.4, 24.5, 26.8, 29.7, 36.9, 38.4, 38.8, 39.8, 45.5, 56.5, 57.1, 116.0, 116.3, 129.0, 131.1, 131.3, 157.1, 173.7, 175.8. HPLC-ELS: 99.8%. HRMS (MALDI): $C_{20}H_{35}N_4O_3$ requires M + 1 at *m*/*z* 379.2709; found 379.2693.

(*S*)-*N*-[5-[(3-Aminopropyl)amino]pentyl]-4-hydroxy-α-[(1-oxobutyl)amino]benzene-propaneamide Bis(trifluoroacetate) (PhTX-53, 10b). Yield: 6%. ^{1}H NMR (CD_3OD): δ 0.86 (t, J = 7.3 Hz, 3H), 1.21−1.72 (m, 10H), 2.17 (t, J = 7.2 Hz, 2H), 2.80 (dd, J = 13.6/8.2, 1H), 2.92−3.22 (m, 9H), 4.42 (t, J = 7.7 Hz, 1H), 6.69 (d, J = 8.5 Hz, 2H), 7.04 (d, J = 8.5 Hz, 2H). ^{13}C NMR: δ 13.7, 19.8, 25.9, 26.2 (2), 37.3, 37.5, 37.8, 38.2, 39.2, 45.2, 46.9, 56.0, 115.4, 115.7, 128.4, 130.5, 130.7, 156.6, 173.1, 175.3. HPLC-ELS: 100.0%. HRMS (MALDI): $C_{21}H_{37}N_4O_3$ requires M + 1 at *m*/*z* 393.2865; found 393.2850.

(*S*)-*N*-[5-[(4-Aminobutyl)amino]pentyl]-4-hydroxy-α-[(1-oxobutyl)amino]benzene-propaneamide Bis(trifluoroacetate) (PhTX-54, 10c). Yield: 10%. ^{1}H NMR (CD_3OD): δ 0.86 (t, J = 7.3 Hz, 3H), 1.22−1.77 (m, 12H), 2.17 (t, J = 7.2 Hz, 2H), 2.79 (dd, J = 13.6/8.1, 1H), 2.92−3.22 (m, 9H), 4.42 (t, J = 7.6 Hz, 1H), 6.69 (d, J = 8.5 Hz, 2H), 7.04 (d, J = 8.5 Hz, 2H). ^{13}C NMR: δ 14.0, 20.4, 24.4, 24.7, 25.7, 26.9, 29.7, 38.4, 38.8, 39.8, 40.1, 48.1, 48.4, 56.8, 116.0, 116.3, 129.0, 131.1, 131.4, 157.2, 173.7, 175.8. HPLC-ELS: 99.9%. HRMS (MALDI): $C_{22}H_{39}N_4O_3$ requires M + 1 at *m*/*z* 407.3022; found 407.3011.

(*S*)-*N*-[5-[(5-Aminopentyl)amino]pentyl]-4-hydroxy-α-[(1-oxobutyl)amino]benzene-propaneamide Bis(trifluoroacetate) (PhTX-55, 10d). Yield: 16%. ^{1}H NMR (CD_3OD): δ 0.86 (t, J = 7.3 Hz, 3H), 1.21−1.79 (m, 14H), 2.17 (t, J = 7.1 Hz, 2H), 2.79 (dd, J = 13.6/8.1, 1H), 2.92−3.22 (m, 9H), 4.43 (t, J = 7.7 Hz, 1H), 6.69 (d, J = 8.5 Hz, 2H), 7.04 (d, J = 8.5 Hz, 2H). ^{13}C NMR: δ 14.1, 20.4, 24.6, 24.7, 26.9 (2), 28.1, 29.7, 38.4, 38.8, 39.8, 40.4, 49.8 (2), 56.7, 116.0, 116.3, 129.0, 131.1, 131.4, 157.1, 173.6, 175.8. HPLC-ELS: 100.0%. HRMS (MALDI): $C_{23}H_{41}N_4O_3$ requires M + 1 at *m*/*z* 421.3178; found 421.3177.

(*S*)-*N*-[5-[(7-Aminoheptyl)amino]pentyl]-4-hydroxy-α-[(1-oxobutyl)amino]benzene-propaneamide Bis(trifluoroacetate) (PhTX-57, 10e). Yield: 19%. ^{1}H NMR (CD_3OD): δ 0.86 (t, J = 7.3 Hz, 3H), 1.18−1.77 (m, 18H), 2.17 (t, J = 7.1 Hz, 2H), 2.79 (dd, J = 13.6/8.1, 1H), 2.89−3.22 (m, 9H), 4.43 (t, J = 7.8 Hz, 1H), 6.69 (d, J = 8.4 Hz, 2H), 7.04 (d, J = 8.4 Hz, 2H).^{13}C NMR: δ 13.8, 20.1, 24.4, 26.6, 27.0 (2), 27.2, 28.3, 29.4, 29.5, 38.1, 38.5, 39.5, 40.4, 48.0, 48.4, 56.5, 115.7, 116.0, 128.7, 130.8, 131.1, 156.7, 173.4, 175.5. HPLC-ELS: 99.9%. HRMS (MALDI): $C_{25}H_{45}N_4O_3$ requires M + 1 at *m*/*z* 449.3491; found 449.3501.

(*S*)-*N*-[5-[(8-Aminooctyl)amino]pentyl]-4-hydroxy-α-[(1-oxobutyl)amino]benzene-propaneamide Bis(trifluoroacetate) (PhTX-58, 10f). Yield: 13%. ^{1}H NMR (CD_3OD): δ 0.86 (t, J = 7.3 Hz, 3H), 1.15−1.73 (m, 20H), 2.17 (t, J = 7.1 Hz, 2H), 2.79 (dd, J = 13.6/8.0, 1H), 2.88−3.21 (m, 9H), 4.42 (t, J = 7.6 Hz, 1H), 6.69 (d, J = 8.5 Hz, 2H), 7.04 (d, J = 8.5 Hz, 2H).^{13}C NMR: δ 13.9, 20.2, 24.4, 26.7, 27.1, 27.3, 27.4, 28.4, 29.5, 29.6, 29.9, 38.2, 38.6, 39.6, 40.5, 48.1, 48.4, 56.6, 115.8, 116.1, 128.8, 130.8, 131.2, 156.9, 173.4, 175.6. HPLC-ELS: 99.5%. HRMS (MALDI): $C_{26}H_{47}N_4O_3$ requires M + 1 at *m*/*z* 463.3648; found 463.3644.

(*S*)-*N*-[5-[(9-Aminononyl)amino]pentyl]-4-hydroxy-α-[(1-oxobutyl)amino]benzene-propaneamide Bis(trifluoroacetate) (PhTX-59, 10g). Yield: 4%. ^{1}H NMR (CD_3OD): δ 0.86 (t, J = 7.4 Hz, 3H), 1.19−1.75 (m, 22H), 2.17 (t, J = 7.2 Hz, 2H), 2.79 (dd, J = 13.7/8.1, 1H), 2.86−3.21 (m, 9H), 4.42 (t, J = 7.6 Hz, 1H), 6.69 (d, J = 8.5 Hz, 2H), 7.04 (d, J = 8.5 Hz, 2H).^{13}C NMR: δ 13.7, 20.1, 24.1, 26.6, 27.2, 27.3, 27.4, 28.4, 29.7, 29.8, 30.0 (2), 38.2, 38.5, 39.5, 40.5, 48.0, 48.1, 56.6, 115.7, 116.0, 128.7, 130.8, 131.0, 156.8, 173.4, 175.9. HPLC-ELS: 98.5%. HRMS (MALDI): $C_{27}H_{49}N_4O_3$ requires M + 1 at *m*/*z* 477.3804; found 477.3794.

(S)-*N*-[5-[(10-Aminodecyl)amino)pentyl]-4-hydroxy-α-[(1-oxobutyl)amino]benzene-propaneamide Bis(trifluoroacetate) (PhTX-5(10), 10h). Yield: 35%. ^{1}H NMR (CD_3OD): δ 0.84 (t, J = 7.4 Hz, 3H), 1.12−1.72 (m, 24H), 2.15 (t, J = 7.4 Hz, 2H), 2.72−3.23 (m, 10H), 4.42 (t, J = 7.8 Hz, 1H), 6.68 and 7.03 (AA′BB′ system, aromatic H, 4H).^{13}C NMR: δ 13.2, 19.4, 23.7, 25.9, 26.4, 26.6, 26.7, 27.7, 28.7, 29.3 (2), 29.5 (2), 37.4, 37.8, 38.9, 39.9, 47.9, 48.0, 55.8, 115.5 (2), 128.0, 130.4 (2), 156.2, 172.6, 174.8. HPLC-ELS: 98.7%. HRMS (MALDI): $C_{28}H_{51}N_4O_3$ requires M + 1 at *m*/*z* 491.3961; found 491.3955.

(S)-*N*-[5-[(12-Aminododecyl)amino)pentyl]-4-hydroxy-α-[(1-oxobutyl)amino]benzene-propaneamide Bis(trifluoroacetate) (PhTX-5(12), 10i). Yield: 36%. ^{1}H NMR (CD_3OD): δ 0.84 (t, J = 7.4 Hz, 3H), 1.10−1.75 (m, 28H), 2.15 (t, J = 7.2 Hz, 2H), 2.70−3.25 (m, 10H), 4.43 (t, J = 8.0 Hz, 1H), 6.87 and 7.16 (AA′BB′ system, aromatic H, 4H).^{13}C NMR: δ 13.1, 19.4, 23.7, 25.9, 26.5, 26.6, 26.7, 27.7, 28.7, 29.3 (2), 29.6 (2), 29.7 (2), 37.4, 37.8, 38.9, 39.8, 47.9, 48.0, 55.8, 115.4 (2), 128.0, 130.4 (2), 156.2, 172.6, 174.8. HPLC-ELS: 99.6%. HRMS (MALDI): $C_{30}H_{55}N_4O_3$ requires M + 1 at *m*/*z* 519.4274; found 519.4280.

(*S*)-*N*-[2-[(6-Aminohexyl)amino]ethtyl]-4-hydroxy-α-[(1-oxobutyl)amino]benzene-propaneamide Bis(trifluoroacetate) (PhTX-26, 13a). Yield: 9%. ^{1}H NMR (CD_3OD): δ 0.87 (t, J = 7.3 Hz, 3H), 1.42−1.76 (m, 10H), 2.18 (t, J = 7.3 Hz, 2H), 2.84 (dd, J = 13.7/8.3, 1H), 2.88−3.15 (m, 9H), 4.30 (t, J = 7.3 Hz, 1H), 6.69 (d, J = 8.6 Hz, 2H), 7.04 (d, J = 8.5 Hz, 2H). ^{13}C NMR: δ 13.7, 20.0, 26.6, 26.9 (2), 28.2, 36.6, 37.4, 38.3, 40.3, 48.0, 48.6, 57.1, 115.7, 116.1, 128.3, 130.7, 131.0, 157.1, 175.0, 176.1. HPLC-ELS: 99.2%. HRMS (MALDI): $C_{21}H_{37}N_4O_3$ requires M + 1 at *m*/*z* 393.2865; found 393.2857.

(*S*)-*N*-[3-[(6-Aminohexyl)amino]propyl]-4-hydroxy-α-[(1-oxobutyl)amino]benzene-propaneamide Bis(trifluoroacetate) (PhTX-36, 13b). Yield: 12%. ^{1}H NMR (CD_3OD): δ 0.88 (t, J = 7.4 Hz, 3H), 1.42−1.84 (m, 12H), 2.18 (t, J = 7.3 Hz, 2H), 2.79−3.00 (m, 8H), 3.13−3.28 (m, 2H), 4.36 (t, J = 7.8 Hz, 1H), 6.69 (d, J = 8.4 Hz, 2H), 7.04 (d, J = 8.4 Hz, 2H).^{13}C NMR: δ 13.8, 20.1, 26.6, 26.8, 26.9, 27.2, 28.2, 36.5, 37.7, 38.4, 40.3, 45.9, 49.5, 56.8, 115.7, 116.1, 128.5, 130.7, 131.0, 157.0, 174.7, 175.8. HPLC-ELS: 98.2%. HRMS (MALDI): $C_{22}H_{39}N_4O_3$ requires M + 1 at *m*/*z* 407.3022; found 407.3015.

(*S*)-*N*-[4-[(6-Aminohexyl)amino]butyl]-4-hydroxy-α-[(1-oxobutyl)amino]benzene-propaneamide Bis(trifluoroacetate) (PhTX-46, 13c). Yield: 13%. ^{1}H NMR (CD_3OD): δ 0.85 (t, J = 7.4 Hz, 3H), 1.39−1.79 (m, 14H), 2.16 (t, J = 7.3 Hz, 2H), 2.80 (dd, J = 13.7/8.5, 1H), 2.89−3.04 (m, 7H), 3.11−3.19 (m, 2H), 4.40 (t, J = 7.0 Hz, 1H), 6.69 (d, J = 8.5 Hz, 2H), 7.04 (d, J = 8.5 Hz, 2H).^{13}C NMR: δ 13.7, 20.1, 24.0, 24.2, 26.8, 26.9, 27.1, 28.1, 38.0, 38.5, 39.0, 40.3, 49.3, 49.4, 56.6, 115.8 (2), 128.6, 130.9 (2), 159.9,

173.7, 175.6. HPLC-ELS: 99.3%. HRMS (MALDI): $C_{23}H_{41}N_4O_3$ requires M + 1 at *m/z* 421.3178; found 421.3175.

(*S*)-*N*-[6-[(6-Aminohexyl)amino]hexyl]-4-hydroxy-α-[(1-oxobutyl)amino]benzene-propaneamide Bis(trifluoroacetate) (PhTX-66, 13d). Yield: 3%. ^{1}H NMR (CD_3OD): δ 0.86 (t, J = 7.3 Hz, 3H), 1.19−1.77 (m, 18H), 2.16 (t, J = 7.1 Hz, 2H), 2.74−3.21 (m, 10H), 4.44 (t, J = 7.3 Hz, 1H), 6.68 (d, J = 8.5 Hz, 2H), 7.03 (d, J = 8.5 Hz, 2H). ^{13}C NMR: δ 13.7, 20.1, 24.0, 26.8 (2), 26.9, 27.2, 28.1, 29.5, 29.8, 38.0, 38.5, 40.0, 40.3, 49.5, 49.6, 56.6, 115.8 (2), 128.6, 130.9 (2), 159.9, 173.2, 175.4. HPLC-ELS: 98.5%. HRMS (MALDI): $C_{25}H_{45}N_4O_3$ requires M + 1 at *m/z* 449.3491; found 449.3494.

(*S*)-*N*-[7-[(6-Aminohexyl)amino]heptyl]-4-hydroxy-α-[(1-oxobutyl)amino]benzene-propaneamide Bis(trifluoroacetate) (PhTX-76, 13e). Yield: 8%. ^{1}H NMR (CD_3OD): δ 0.86 (t, J = 7.3 Hz, 3H), 1.17−1.77 (m, 20H), 2.16 (t, J = 7.1 Hz, 2H), 2.78 (dd, J = 13.67/8.2, 1H), 2.84−3.21 (m, 9H), 4.45 (t, J = 7.2 Hz, 1H), 6.68 (d, J = 8.5 Hz, 2H), 7.03 (d, J = 8.5 Hz, 2H). ^{13}C NMR: δ 13.7, 20.1, 24.0, 26.8, 26.9 (2), 27.2, 27.3, 28.2, 29.5, 29.9, 38.2, 38.5, 40.0, 40.3, 49.5, 49.6, 56.4, 115.8 (2), 128.7, 130.9 (2), 159.9, 173.2, 175.4. HPLC-ELS: 99.4%. HRMS (MALDI): $C_{26}H_{47}N_4O_3$ requires M + 1 at *m/z* 463.3648; found 463.3655.

(*S*)-*N*-[8-[(6-Aminohexyl)amino]octyl]-4-hydroxy-α-[(1-oxobutyl)amino]benzene-propaneamide Bis(trifluoroacetate) (PhTX-86, 13f). Yield: 6%. ^{1}H NMR (CD_3OD): δ 0.85 (t, J = 7.3 Hz, 3H), 1.18−1.76 (m, 22H), 2.16 (t, J = 7.2 Hz, 2H), 2.77 (dd, J = 13.5/8.1, 1H), 2.88−3.20 (m, 9H), 4.46 (t, J = 7.1 Hz, 1H), 6.68 (d, J = 8.5 Hz, 2H), 7.03 (d, J = 8.5 Hz, 2H).^{13}C NMR: δ 13.7, 20.1, 24.0, 26.8, 26.9, 27.0, 27.3, 27.4, 28.1, 28.2, 29.8, 30.0, 38.2, 38.5, 40.0, 40.3, 49.4 (2), 56.3, 115.8 (2), 128.7, 130.9 (2), 156.9, 173.2, 175.4. HPLC-ELS: 99.7%. HRMS (MALDI): $C_{27}H_{49}N_4O_3$ requires M + 1 at *m/z* 477.3804; found 477.3783.

(*S*)-*N*-[9-[(6-Aminohexyl)amino]nonyl]-4-hydroxy-α-[(1-oxobutyl)amino]benzene-propaneamide Bis(trifluoroacetate) (PhTX-96, 13g). Yield: 5%. ^{1}H NMR (CD_3OD): δ 0.85 (t, J = 7.3 Hz, 3H), 1.17−1.77 (m, 24H), 2.15 (t, J = 7.1 Hz, 2H), 2.77 (dd, J = 13.7/8.4, 1H), 2.89−3.20 (m, 9H), 4.46 (t, J = 7.1 Hz, 1H), 6.68 (d, J = 8.5 Hz, 2H), 7.03 (d, J = 8.5 Hz, 2H).^{13}C NMR: δ 13.7, 20.1, 26.8, 26.9 (2), 27.1, 27.3, 27.6, 28.2, 29.9, 30.0 (2), 30.1, 38.2, 38.5, 40.1, 40.3, 49.7, 49.9, 56.2, 115.8 (2), 128.7, 130.9 (2), 156.9, 173.2, 175.4. HPLC-ELS: 99.6%. HRMS (MALDI): $C_{28}H_{51}N_4O_3$ requires M + 1 at *m/z* 491.3961; found 491.3946.

PhTX-83 Analogues. PhTX-38 (**14a**), PhTX-47 (**14b**), PhTX-65 (**14c**), PhTX-74 (**14d**), PhTX-83 (**3**), and PhTX-92 (**14e**) were prepared by Kroman et al.[20]

In Vitro cRNA Transcription. The construct AMPAR1 flop was inserted in the pGEMHE oocyte expression vector. DNA (1 μg) was linearized using the appropriate enzyme. Runoff transcription was performed using MEGAscript Kit (Ambion inc.).

Electrophysiology. A female *Xenopus laevis* frog was anesthetized in a 0.2% MS 222 (3-aminobenzoic acid ethyl ester, Sigma-Aldrich) for 15−30 min, and three to five ovarian lobes were surgically removed. The follicle layer was removed by washing twice in Barth's saline (88.0 mM NaCl, 1.0 mM KCl, 2.4 mM $NaHCO_3$, 15.0 mM HEPES pH 7.5, 0.30 mM $Ca(NO_3)_2$, 0.41 mM $CaCl_2$, 0.82 mM $MgSO_4$, 100 U/mL penicillin), once in OR-2 (82.5 mM NaCl, 2.0 mM KCl, 1.0 mM $MgCl_2$, 5.0 mM HEPES pH 7.5) followed by treatment with collagenase A (1 mg/mL in OR-2) for 2−3 h at RT. Oocytes at stage four to five were selected and injected the following day with 50 nl (5−50 ng) of cRNA. The oocytes were kept at 18 °C in Barth's saline before recordings were performed 4 to 7 days after injection, using a two-electrode voltage clamp (Warner OC-725C; Warner Instruments, Inc., Hamden, CT). The recording solution was low Ca^{2+} Ringer (LCR; 115 mM NaCl, 0.1 mM $CaCl_2$, 2.5 mM KCl, 1.8 mM $MgCl_2$ and 10mM HEPES pH 7.5). The LCR buffer was chosen to prevent activation of the endogenous Ca^{2+}-activated Cl^- channels. The oocytes were clamped at −70 mV. Electrodes (borosilicate glass capillaries, outer diameter, 1.5 mm; inner diameter, 1.17 mm; with inner filament; Harvard apparatus LTD, Kent, UK) were filled by 3 M KCl and exhibited resistance around 0.5 MΩ.

Data Analysis. The data were acquired using Clampex 8.0 (Axon instruments, Inc., Union City, CA). All responses were normalized to the average of a glutamate response applied before and after the channel blocker and glutamate coapplication. Normalized responses in the interval [0.4;0.6] were used to calculate the K_i (equilibrium dissociation constant) for the channel blocker. At high glutamate concentration (we use 100 μM) where all the ion-channels are open, the proportion of ion-channels occupied by the channel blocker will be given by the Hill−Langmuir equation. We assume that the philanthotoxins block the ion-channel in the re-entrant loop region and therefore will have minor effects on the equilibrium constants between the inactive, active and desensitized states. Hence, the equilibrium dissociation constants for the Philanthotoxins will be: $K_i = ([PhTX] \times I_{Normal})/(1 - I_{Normal})$. Mean and SD values were calculated assuming a Gaussian distribution of K_i.

"Native" AMPA Receptor Assay. A two-electrode voltage clamp (TEVC) was used to record responses of *X. laevis* oocytes expressing AMPA receptors to 100 μM kainate. *X. laevis* oocytes were injected with rat brain RNA and incubated at 18 °C for at least 3 days in saline containing 96 mM NaCl, 2 mM KCl, 1 mM $MgCl_2$, 1.8 mM $CaCl_2$, 2.5 mM Na-pyruvate, 0.5 mM theophylline, 50 mg/mL gentamicin, 5 mM HEPES (pH 7.5). Single oocytes were transferred to a perfusion bath and continuously washed with saline containing 95 mM NaCl, 2 mM KCl, 2 mM $CaCl_2$, and 5 mM HEPES (pH 7.5 with NaOH). Microelectrodes were pulled from borosilicate glass capillaries (GC150TF-10, Clark Electromedical Instruments) using a Sutter P-97 programmable puller and had resistances of ∼0.5 MΩ when filled with 3.0 M KCl. The oocytes were voltage clamped at −80 mV (unless otherwise stated) using an Axoclamp 2A (Axon Instruments), and output currents were transferred to a PC via a Digidata 1200 interface (Axon Instruments) and WinEDR software (Dr John Dempster, Department of Physiology and Pharmacology, University of Strathclyde, UK). Responses of AMPAR were elicited by perfusion of 100 μM kainic acid until a plateau current was achieved, then philanthotoxins (**3**, **4**, **10a-10i**, **13a**−**g**, and **14a-14e**) were coapplied, with stepwise increases in their concentration until a new plateau current was obtained. Currents were measured at each plateau using WinEDR software (Dr. John Dempster, Department of Physiology and Pharmacology, University of Strathclyde, UK) and analyzed with Graphpad Prism 4 software. Data were plotted as philanthotoxin concentration versus % inhibition for at least 3 oocytes per concentration, and IC_{50}'s determined by fitting with the equation:

$$\% \text{ inhibition} = 100/(1 + (IC_{50}/[PhTX])^S)$$

where [PhTX] is the philanthotoxin concentration and S is the Hill slope.

Molecular Modeling. Molecular modeling was performed using the ZMM program package (www.zmmsoft.com). The AMBER force field[43] and the Monte Carlo with energy minimization (MCM) strategy[44] were used to find low-energy equilibrium conformations of ligand−channel complexes within internal coordinates. All torsional and bond angles of ligands were treated as variables. The atomic charges of ligands were calculated by the AM1 method[45] using the MOPAC program. The hydration energy was calculated by the implicit-solvent method.[46] Flat-bottom energy penalty functions (constraints) were used for homology modeling of the channel and for ligand docking. The pin constraints limit deviation of α-carbons from their position in template structure; the upper limit of the free deviation was 1 Å. The distance constraints limit the distance between two atoms and were used to preserve specific interactions; the upper limit for distance constraints was 2.5 Å. For other details of calculations see ref 37.

Acknowledgment. We thank the Alfred Benzon Foundation for financial support (to J.K.N). Technical assistance from Ms. Dorthe Kroghave Toftdahl and Mr. Erik Damgård, Department of Spectroscopy, Medicinal Chemistry Research, H. Lundbeck A/S, is appreciated.

Supporting Information Available: Four tables listing IC_{50} and K_i values for compounds **3**, **4**, **10a**−**i**, **13a**−**g**, **14a**−**e**. This material is available free of charge via the Internet at http://pubs.acs.org.

References

(1) Bliss, T. V. P.; Collingridge, G. L. A synaptic model of memory: long-term potentiation in the hippocampus. *Nature* **1993**, *361*, 31−39.

(2) Malenka, R. C.; Nicoll, R. A. Long-term potentiation − a decade of progress? *Science* **1999**, *285*, 1870−1874.

(3) Kemp, N.; Bashir, Z. I. Long-term depression: a cascade of induction and expression mechanisms. *Prog. Neurobiol.* **2001**, *65*, 339−365.

(4) Dingledine, R.; Borges, K.; Bowie, D.; Traynelis, S. F. The glutamate receptor ion channels. *Pharmacol. Rev.* **1999**, *51*, 7−61.

(5) Ozawa, S.; Kamiya, H.; Tsuzuki, K. Glutamate receptors in the mammalian central nervous system. *Prog. Neurobiol.* **1998**, *54*, 581−618.

(6) Bräuner-Osborne, H.; Egebjerg, J.; Nielsen, E. Ø.; Madsen, U.; Krogsgaard-Larsen, P. Ligands for glutamate receptors: design and therapeutic prospects. *J. Med. Chem.* **2000**, *43*, 2609−2645.

(7) Ferris, S. H. Evaluation of memantine for the treatment of Alzheimer's disease. *Expert Opin. Pharmacother.* **2003**, *4*, 2305−2313.

(8) Bredt, D. S.; Nicoll, R. A. AMPA receptor trafficking at excitatory synapses. *Neuron* **2003**, *40*, 361−379.

(9) Song, I.; Huganir, R. L. Regulation of AMPA receptors during synaptic plasticity. *Trends Neurosci.* **2002**, *25*, 578−588.

(10) Malinow, R.; Malenka, R. C. AMPA receptor trafficking and synaptic plasticity. *Annu. Rev. Neurosci.* **2002**, *25*, 103−126.

(11) Carroll, R. C.; Beattie, E. C.; von Zastrow, M.; Malenka, R. C. Role of AMPA receptor endocytosis in synaptic plasticity. *Nature Rev. Neurosci.* **2001**, *315*−*324*.

(12) Bleakman, D.; Lodge, D. Neuropharmacology of AMPA and kainate receptors. *Neuropharmacology* **1998**, *37*, 1187−1204.

(13) Weiss, J. H.; Sensi, S. L. Ca^{2+}-Zn^{2+} permeable AMPA or kainate receptors: possible key factors in selective neurodegeneration. *Trends Neurosci.* **2000**, *23*, 365−371.

(14) Pellegrini-Giampietro, D. E.; Gorter, J. A.; Bennet, M. V. L.; Zukin, R. Z. The GluR2 (GluR−B) hypothesis: Ca^{2+}-permeable AMPA receptors in neurological disorders. *Trends Neurosci.* **1997**, *20*, 464−470.

(15) Gill, R.; Lodge, D. Pharmacology of AMPA antagonists and their role in neuroprotection. *Int. Rev. Neurobiol.* **1997**, *40*, 197−232.

(16) Mellor, I. R.; Usherwood, P. N. R. Targeting ionotropic receptors with polyamine-containing toxins. *Toxicon* **2004**, *43*, 493−508.

(17) Strømgaard, K.; Mellor, I. R. AMPA receptor ligands: synthetic and pharmacological studies of polyamines and polyamine toxins. *Med. Res. Rev.* **2004**, *24*, 589−620.

(18) Strømgaard, K.; Andersen, K.; Krogsgaard-Larsen, P.; Jaroszewski, J. W. Recent advances in the medicinal chemistry of polyamine toxins. *Minirev. Med. Chem.* **2001**, *1*, 317−338.

(19) Eldefrawi, A. T.; Eldefrawi, M. E.; Konno, K.; Mansour, N. A.; Nakanishi, K.; Oltz, E.; Usherwood, P. N. R. Structure and synthesis of a potent glutamate receptor antagonist in wasp venom. *Proc. Natl. Acad. Sci. U.S.A.* **1988**, *85*, 4910−4913.

(20) Kromann, H.; Krikstolaityte, S.; Andersen, A. J.; Andersen, K.; Krogsgaard-Larsen, P.; Jaroszewski, J. W.; Egebjerg, J.; Strømgaard, K. Solid-phase synthesis of polyamine toxin analogues: potent and selective antagonists of Ca^{2+}-permeable AMPA receptors. *J. Med. Chem.* **2002**, *45*, 5745−5754.

(21) Mellor, I. R.; Brier, T. J.; Pluteanu, F.; Strømgaard, K.; Saghyan, A.; Eldursi, N.; Brierley, M. J.; Andersen, K.; Jaroszewski, J. W.; Krogsgaard-Larsen, P.; Usherwood, P. N. R. Modification of the philanthotoxin-343 polyamine moiety results in different structure−activity profiles at muscle nicotinic ACh, NMDA and AMPA receptors. *Neuropharmacology* **2003**, *44*, 70−80.

(22) Lees, G. J. Pharmacology of AMPA/kainate receptor ligands and their therapeutic potential in neurological and psychiatric disorders. *Drugs* **2000**, *59*, 33−78.

(23) Kuner, R.; Groom, A. J.; Bresink, I.; Kornau, H. C.; Stefovska, V.; Müller, G.; Hartmann, B.; Tschauner, K.; Waibel, S.; Ludolph, A. C.; Ikonomidou, C.; Seeburg, P. H.; Turski, L. Late-onset motoneuron disease caused by a functionally modified AMPA receptor subunit. *Proc. Natl. Acad. Sci. U.S.A.* **2005**, *102*, 5826−5831.

(24) Kawahara, Y.; K., I.; Sun, H.; Aizawa, H.; Kanazawa, I.; Kwak, S. RNA editing and death of motor neurons. *Nature* **2004**, *427*, 801.

(25) Kwak, S.; Kawahara, Y. Deficient RNA editing of GluR2 and neuronal death in amyotropic lateral sclerosis. *J. Mol. Med.* **2005**, *83*, 110−120.

(26) Wollmuth, L. P.; Sobolevsky, A. I. Structure and gating of the glutamate receptor ion channel. *Trends Neurosci.* **2004**, *27*, 321−328.

(27) Madden, D. R. The inner workings of the AMPA receptors. *Curr. Opin. Drug. Discovery Dev.* **2002**, *5*, 741−748.

(28) Kuner, T.; Seeburg, P. H.; Guy, H. R. A common architecture for K^+ channels and ionotropic glutamate receptors? *Trends Neurosci.* **2003**, *26*, 27−32.

(29) Tikhonov, D. B.; Zhorov, B. S.; Magazanik, L. G. Intersegment hydrogen bonds as possible structural determinants of the N/Q/R site in glutamate receptors. *Biophys. J.* **1999**, *77*, 1914−1926.

(30) Jørgensen, M. R.; Olsen, C. A.; Mellor, I. R.; Usherwood, P. N.; Witt, M.; Franzyk, H.; Jaroszewski, J. W. The effects of conformational constraints and steric bulk in the amino acid moiety of philanthotoxins on AMPAR antagonism. *J. Med. Chem.* **2005**, *48*, 56−70.

(31) Strømgaard, K.; Jensen, L. S.; Vogensen, S. B. Polyamine toxins: development of selective ligands for ionotropic receptors. *Toxicon* **2005**, *45*, 249−254.

(32) Strømgaard, K.; Andersen, K.; Ruhland, T.; Krogsgaard-Larsen, P.; Jaroszewski, J. W. A versatile method for solid-phase synthesis of polyamines: neuroactive polyamine toxins as example. *Synthesis* **2001**, 877−884.

(33) Tikhonov, D. B.; Mellor, I. R.; Usherwood, P. N.; Magazanik, L. G. Modeling of the pore domain of the GluR1 channel: Homology with K^+ channel and binding of channel blockers. *Biophys. J.* **2002**, *82*, 1884−1893.

(34) Doyle, D. A.; Morais Cabral, J.; Pfuetzner, R. A.; Kuo, A.; Gulbis, J. M.; Cohen, S. L.; Chait, B. T.; MacKinnon, R. The structure of the potassium channel: molecular basis of K^+ conduction and selectivity. *Science* **1998**, *280*, 69−77.

(35) Jiang, Y.; Lee, A.; Chen, J.; Cadene, M.; Chait, B. T.; MacKinnon, R. The open pore conformation of potassium channels. *Nature* **2002**, *417*, 523−526.

(36) Zhorov, B. S.; Tikhonov, D. B. Potassium, sodium, calcium and glutamate-gated channels: pore architecture and ligand action. *J. Neurochem.* **2004**, *88*, 782−799.

(37) Tikhonov, D. B.; Zhorov, B. S. Modeling P-loops domain of sodium channel: homology with potassium channels and interaction with ligands. *Biophys. J.* **2005**, *88*, 184−197.

(38) Tikhonov, D. B.; Magazanik, L. G.; Mellor, I. R.; Usherwood, P. N. R. Possible influence of intramolecular hydrogen bonds on the three-dimensional structure of polyamine amides and their interaction with ionotropic receptors. *Receptors Channels* **2000**, *7*, 227−236.

(39) G+2 refer to the oxygen from backbone carbonyl of a glycine (G) residue located two residues downstream from the Q/R-site.

(40) Bolshakov, K. V.; Tikhonov, D. B.; Gmiro, V. E.; Magazanik, L. G. Different arrangement of hydrophobic and nucleophilic components of channel binding sites in *N*-methyl-D-aspartate and AMPA receptors of rat brain is revealed by channel blockade. *Neurosci. Lett.* **2000**, *291*, 101−104.

(41) Bolshakov, K. V.; Kim, K. H.; Potapjeva, N. N.; Gmiro, V. E.; Tikhonov, D. B.; Usherwood, P. N. R.; Mellor, I. R.; Magazanik, L. G. Design of antagonists for NMDA and AMPA receptors. *Neuropharmacology* **2005**, *49*, 144−155.

(42) Woodhull, A. M. Ionic blockage of sodium channels in nerve. *J. Gen. Physiol.* **1973**, *61*, 687−708.

(43) Weiner, S. J.; Kollman, P. A.; Case, D. A.; Singh, U. C.; Chio, C.; Alagona, G.; Profeta, S.; Weiner, P. K. A new force field for molecular mechnical simulation of nucleic acids and proteins. *J. Am. Chem. Soc.* **1984**, *106*, 765−784.

(44) Li, Z.; Scheraga, H. A. Monte Carlo-minimization approach to the multiple-minima problem in protein folding. *Proc. Natl. Acad. Sci. U.S.A.* **1987**, *84*, 6611−6615.

(45) Dewar, M. J. S.; Zoevisch, E. G.; Healy, E. F.; Stewart, J. J. AM1: a new general purpose quantum mechanical model. *J. Am. Chem. Soc.* **1985**, *107*, 3902−3909.

(46) Lazaridis, T.; Karplus, M. Effective energy function for proteins in solution. *Proteins* **1999**, *35*, 133−152.

JM060606J